ADVANCING EARTH AND SPACE SCIENCES

Space Weather

RESEARCH ARTICLE
10.1029/2025SW004441

Solar Cycle and Seasonal Dependences of Field-Aligned Currents

Rajkumar Hajra[1], Bruce T. Tsurutani[4], Quanming Lu[1], Aimin Du[2], San Lu[1], and Ezequiel Echer[3]

[1]CAS Key Laboratory of Geospace Environment, School of Earth and Space Sciences, University of Science and Technology of China, Hefei, People's Republic of China, [2]College of Earth and Planetary Sciences, Chinese Academy of Sciences, Beijing, People's Republic of China, [3]DIHPA/CGCE, Instituto Nacional de Pesquisas Espaciais, São José dos Campos, Brazil, [4]Retired, Pasadena, CA, USA

Key Points:

- Long-term variations of field-aligned currents (FACs) are studied using ∼15-yearlong FAC measurements
- FACs exhibit maximum and minimum intensities ∼1 year after the solar activity cycle maximum and minimum phases, respectively
- Ionospheric conductance-driven dayside FACs exhibit a summer peak, nightside FACs are driven by solar wind-magnetosphere energy coupling

Correspondence to:

R. Hajra,
rhajra@ustc.edu.cn;
rajkumarhajra@yahoo.co.in

Citation:

Hajra, R., Tsurutani, B. T., Lu, Q., Du, A., Lu, S., & Echer, E. (2025). Solar cycle and seasonal dependences of field-aligned currents. *Space Weather*, *23*, e2025SW004441. https://doi.org/10.1029/2025SW004441

Received 14 MAR 2025
Accepted 8 MAY 2025

Author Contributions:

Conceptualization: Rajkumar Hajra, Bruce T. Tsurutani
Data curation: Rajkumar Hajra
Formal analysis: Rajkumar Hajra
Funding acquisition: Rajkumar Hajra
Investigation: Rajkumar Hajra
Methodology: Rajkumar Hajra
Resources: Rajkumar Hajra
Supervision: Rajkumar Hajra, Bruce T. Tsurutani
Validation: Rajkumar Hajra
Visualization: Rajkumar Hajra
Writing – original draft: Rajkumar Hajra
Writing – review & editing: Rajkumar Hajra, Bruce T. Tsurutani, Quanming Lu, Aimin Du, San Lu, Ezequiel Echer

Abstract Enhancements of Birkeland field-aligned currents (FACs) have been reported during magnetospheric substorms and geomagnetic storms. While FACs related to geomagnetic disturbances have been extensively studied, the long-term variations of FACs remain less explored. Here, based on ∼15 years of FAC measurements from the Active Magnetosphere and Planetary Electrodynamics Response Experiment, we present quantitative studies on the solar cycle and seasonal dependences of FACs. Yearly mean FACs (both dayside and nightside) are found to increase with increasing $F_{10.7}$ solar flux, peaking ∼1 year after the $F_{10.7}$ maximum and reaching a minimum ∼1 year after the $F_{10.7}$ minimum, with a maximum-to-minimum FAC ratio of ∼2–3. The dayside FAC distributions (median) are characterized by a summer hemispheric peak, ∼99% and ∼35%–38% stronger than in local winter and equinoxes, respectively, while the nightside FAC in winter is only ∼14%–17% weaker than in other seasons. These seasonal patterns are consistent across all years and levels of solar activity. Nightside FACs show a strong correlation (with Spearman's rank correlation coefficients $r = 0.78$–0.82) with solar wind-magnetosphere energy coupling functions, the association is weaker ($r = 0.58$–0.61) for dayside FACs. These results plausibly indicate that the contribution of ionospheric conductivity dominates dayside FACs. Nightside FACs, with weaker ionospheric conductivity contributions, are "directly driven" by energy coupling processes. These findings, based on long-term observations, will be valuable for improving FAC modeling.

Plain Language Summary Geomagnetic field-aligned currents (FACs) flowing around the poles of the Earth are an important aspect of the solar wind-magnetosphere-ionosphere coupling. FACs are known to be enhanced during geomagnetic disturbances. Here we study long-term variations of FACs, their dependences on the solar activity cycle and seasons using a ∼15 yearlong FAC database. FACs exhibit a clear solar cycle dependence, exhibiting the maximum and minimum intensities following the solar activity maximum and minimum, respectively. Dayside FACs largely contributed by ionospheric conductivity variations exhibit the strongest and weakest intensities during local summer and winter, respectively. Nightside FACs, with lesser contribution from ionospheric conductance, exhibit strong association with solar wind-magnetosphere energy coupling.

1. Introduction

The purpose of this work is to study solar cycle and seasonal dependences of Birkeland field-aligned currents (FACs; Birkeland, 1908, 1913). We use the northern and southern hemispheric FAC measurements by the Active Magnetosphere and Planetary Electrodynamics Response Experiment (AMPERE; Anderson et al., 2002, 2021; Waters et al., 2001, 2020) for ∼15 years, from 2 October 2009 through 31 July 2024, along with near-Earth solar wind measurements for this study.

Theoretical prediction of FACs by Birkeland (1908, 1913) and their first measurements by the polar orbiting satellite 1963 38C (Cummings & Dessler, 1967; Zmuda et al., 1966) were followed by the epic works of Iijima and Potemra (1976a, 1976b, 1978) establishing the large-scale morphological features of FACs. FACs consist of two pairs of upward and downward currents along auroral-zone geomagnetic fields, closing through ionospheric horizontal Pedersen currents. The poleward/region 1 currents, downward in the dawn sector and upward in the dusk sector, close through the dayside magnetopause (Chapman & Ferraro, 1931) current and the magnetotail (Ness, 1965; Speiser & Ness, 1967) current. The equatorward/region 2 currents with opposite polarity close through inner magnetospheric partial ring currents (Crooker & McPherron, 1972; Cummings, 1966; Fukushima & Kamide, 1973).

Recent studies have been focused on the relationship between FACs and geomagnetic disturbances, and their solar and interplanetary drivers. Coxon et al. (2014a) reported an increase in FAC magnitude during the substorm expansion phase by ∼1 MA, driven by dayside magnetopause reconnection (Coxon et al., 2014b). FAC magnitude is found to maximize ∼40 min after the onset of geomagnetic storms driven by corotating interaction regions (CIRs) (Pedersen et al., 2021), and ∼1 hr after the onset of storms driven by interplanetary coronal mass ejections (ICMEs) (Pedersen et al., 2022). Wang et al. (2006) reported FAC intensification during the extreme storms in October and November 2003 by a factor of 5 compared to quiet time FAC intensities. Analyses of global FAC maps during two recent storms, April 2023 SYM-H = −233 nT storm (Hajra, Tsurutani, Lu, et al., 2024) and May 2024 SYM-H = −518 nT storm (Hajra, Tsurutani, Lakhina, et al., 2024; Wang et al., 2024), revealed storm-related FACs expanding down to ∼50° magnetic latitude, and FAC intensification by a factor of ∼10 than quiet time values.

Although FACs related to geomagnetic disturbances have been studied extensively, less explored are long-term variation FACs. In an iconic work, Fujii et al. (1981) explored TRIAD satellite records during 1973, 1974, 1976, and 1977 to study seasonal features of the northern hemispheric FACs. Coxon et al. (2016) studied FAC seasonal and diurnal variations using the northern and southern hemispheric FAC measurements made by AMPERE from 2010 through 2015. From these studies, dayside FACs were found to be stronger during summer than during winter by a factor of ∼2, while nightside FACs did not show any significant differences from summer to winter (Fujii et al., 1981). These results can be explained by seasonal differences in ionospheric conductance. Wang et al. (2005) studied the influence of the solar illumination-induced ionospheric conductivity in the southern hemispheric FACs based on 2 years of the Challenging Minisatellite Payload (CHAMP) magnetic field data. Their observations revealed more than a factor of 2 enhancement of the FAC densities for sunlit compared with darkness. However, Coxon et al. (2016) reported more current flows in the northern hemisphere than the southern hemisphere, which could not be explained by variations in ionospheric conductance.

In this paper, we expand on previous studies by using a significantly larger FAC database and including measurements from both hemispheres. The present observations spanning a ∼1.5 solar cycle interval is suitable for understanding the long-term variations of FACs. In addition to a study of FAC seasonal dependences, this long-term database will be used to study, for the first time, solar cycle dependence of FACs, if any. The major questions addressed in this work are: (a) do FAC seasonal features vary with solar cycle phases?, (b) do FACs exhibit solar cycle phase dependence?, and (c) are the long-term FAC variation trends related to solar wind-magnetosphere energy coupling processes? This study is aimed at increasing our understanding of long-term variability of FACs, their underlying physical processes, and potentially leading to the development of predictive FAC models.

2. Data and Methods

The FAC data studied in this work are obtained from the AMPERE Science Data Center of the Johns Hopkins Applied Physics Laboratory (https://ampere.jhuapl.edu/). For the present work, we have used daily data files containing integrated FACs at 2 min time resolution, and their upward ($\mathrm{FAC_{up}}$) and downward ($\mathrm{FAC_{down}}$) components, separately for dayside and nightside currents in the northern and southern hemispheres. Total FACs have been estimated as $\mathrm{FAC_{total}} = (\mathrm{FAC_{up}}–\mathrm{FAC_{down}})/2$. Considering separate FAC measurements for the two hemispheres, February to April months are classified as northern hemispheric spring and southern hemispheric fall equinoxes; May to July as northern hemispheric summer and southern hemispheric winter solstices; August to October as northern hemispheric fall and southern hemispheric spring equinoxes; and November to January as winter in northern hemisphere and summer in southern hemisphere.

The near-Earth solar wind plasma and interplanetary magnetic field (IMF) parameters are obtained from NASA's OMNIWeb Plus database (https://omniweb.gsfc.nasa.gov/) (King & Papitashvili, 2020). The 1-min resolution data are utilized to estimate the following solar wind-magnetosphere coupling functions. The Newell coupling function N_{CF}, estimated as $V_p^{4/3} B_{\mathrm{yz}}^{2/3} \sin^{8/3}(\theta/2)$, is assumed to give an empirical estimate of the rate at which open magnetic fluxes at the magnetopause are closed (Newell et al., 2007). $\Phi_D = 3.2 \times 10^5 V_p^{4/3} B_{\mathrm{yz}} \sin^{9/2}(\theta/2)$ estimates the rate of dayside magnetopause reconnection (Milan et al., 2012). The Akasofu ε-paremeter, $\varepsilon = V_p B_0^2 \sin^4(\theta/2) R_{\mathrm{CF}}^2$, where $R_{\mathrm{CF}} = \left(2B_E^2/\left(\mu_0 m_p N_p V_p^2\right)\right)^{1/6} R_E$ (Chapman & Ferraro, 1931), gives an empirical estimate of magnetospheric energy input rate (Perreault & Akasofu, 1978). In the above expressions, V_p is the solar wind proton speed, N_p is the proton density, m_p is the proton mass, B_0 is the magnitude of IMF, B_x, B_y, and B_z are IMF components, $B_{yz} = \sqrt{B_y^2 + B_z^2}$, θ is the IMF clock angle, B_E is the equatorial geomagnetic field intensity on the surface of the Earth, μ_0 is the free space permeability, and R_E is the Earth's radius. VB_s is the motional/reconnection electric field, where $V = V_p$, and B_s is the IMF southward component (Burton et al., 1975; Finch et al., 2008; Tsurutani et al., 1992).

We computed distributions of FACs by dividing the minimum-to-maximum FAC range into small bins, and counted the numbers of observations for each bin. The distributions are expressed as percentages of total observation counts. The statistical difference of two distributions is estimated by the two-tailed probability factor p (Reiff, 1990). As the distributions are found to be non-normal, the nonparametric Mann Whitney Wilcoxon test/Wilcoxon Rank Sum test (Gibbons & Chakraborti, 2011) is used for the calculating the p-values.

The relationships between the coupling functions and FAC parameters are assessed based on computations of Spearman's rank correlation coefficients. This non-parametric test is more appropriate than the traditional (Pearson's) correlation analysis, as the data exhibit nonlinearity or non-normal distributions. The statistical significance of the correlation coefficients are verified by the Student's t-test (Student, 1908).

The solar cycle is characterized by the $F_{10.7}$ solar fluxes (daily mean), obtained from the Laboratory for Atmospheric and Space Physics (LASP) Interactive Solar Irradiance Data Center (https://lasp.colorado.edu/lisird/).

3. Results

Figure 1 shows variations of daily and monthly mean dayside total FACs (FAC_{day}) in the northern and southern hemispheres along with solar wind-magnetosphere coupling functions N_{CF}, Φ_D, ε, VB_s, and the $F_{10.7}$ solar fluxes during 2009 through 2024.

As clear from the $F_{10.7}$ variation (Figure 1g), the period of this study includes the complete solar cycle 24 (from 2009 through 2019) and the ascending to maximum phases of solar cycle 25 (from 2020 through 2024). While the coupling functions exhibit small-scale fluctuations (Figures 1c–1f), FACs are found to exhibit an annual variation (Figures 1a and 1b). The latter is confirmed by a strong peak at ~12 months in the Lomb-Scargle (Lomb, 1976; Scargle, 1982) power spectra of FAC_{day} (see Appendix A Figure A1). No such annual variation is observed in the coupling functions (not shown). This result plausibly indicates that the long-term trends in FAC_{day} are not driven by solar winds. This will be discussed later in this paper.

The long-term trends of FACs are further explored in Figure 2. The analyses include both dayside and nightside FACs in the northern and southern hemisphers separately. Figure 2b shows the year-month contour of monthly mean FAC_{day} in the northern hemisphere. The contour plot presentation is suitable to identify any year-to-year or solar cycle variation of FAC seasonal features, as well as month-to-month or seasonal variation of solar cycle variation of FACs, if any. Three prominent FAC_{day} peaks are recorded: during July 2012, August 2015, and May 2024. While the 2024 peak corresponds to the ascending phase or the maximum of solar cycle 25 (note that it is not yet known if the solar cycle 25 peak has occurred or not), the 2012 peak preceeds and the 2015 peak follows the solar cycle 24 peak (during 2014). When averaged over all months in a year, that is, the yearly mean northern hemispheric FAC_{day} is found to increase with increasing $F_{10.7}$ from solar minimum during 2009, exhibits a minor peak during 2012 followed by a decrease during 2013 (Figure 2g). The strongest FAC_{day} peak is observed during 2015, ~1 year after the $F_{10.7}$ peak during 2014. While the FAC_{day} decreases after 2015, the entire descending phase upto 2017 is characterized by strong FAC_{day} values. The FAC_{day} minimum is observed during 2020, well after the $F_{10.7}$ minimum during 2019. Considering yearly mean FAC_{day} values, the maximum-to-minimum FAC_{day} ratio is ~2.7. This indicates significant (~170%) solar cycle variation of FAC_{day}, which varies from one season to the other (see Appendix B, Figure B1 and Table B1).

For all years shown in Figure 2b, while the FAC_{day} peak occurrence varies from year to year, the May-July interval (northern hemispheric summer) is characterized by the strongest FAC_{day} values on average over all years (Figure 2a shows monthly FACs, that is, the FAC intensities in each month averaged for all years). On both sides of the summer peak, gradual decreases can be noted in the FAC_{day} intensity during spring and fall equinoxes, with the weakest FAC_{day} during winter months. On average, the summer FAC_{day} is ~2.3 times (~130% stronger than) the winter minimum value. The summer-to-winter (maximum-to-minimum) ratio/asymmetry is consistently

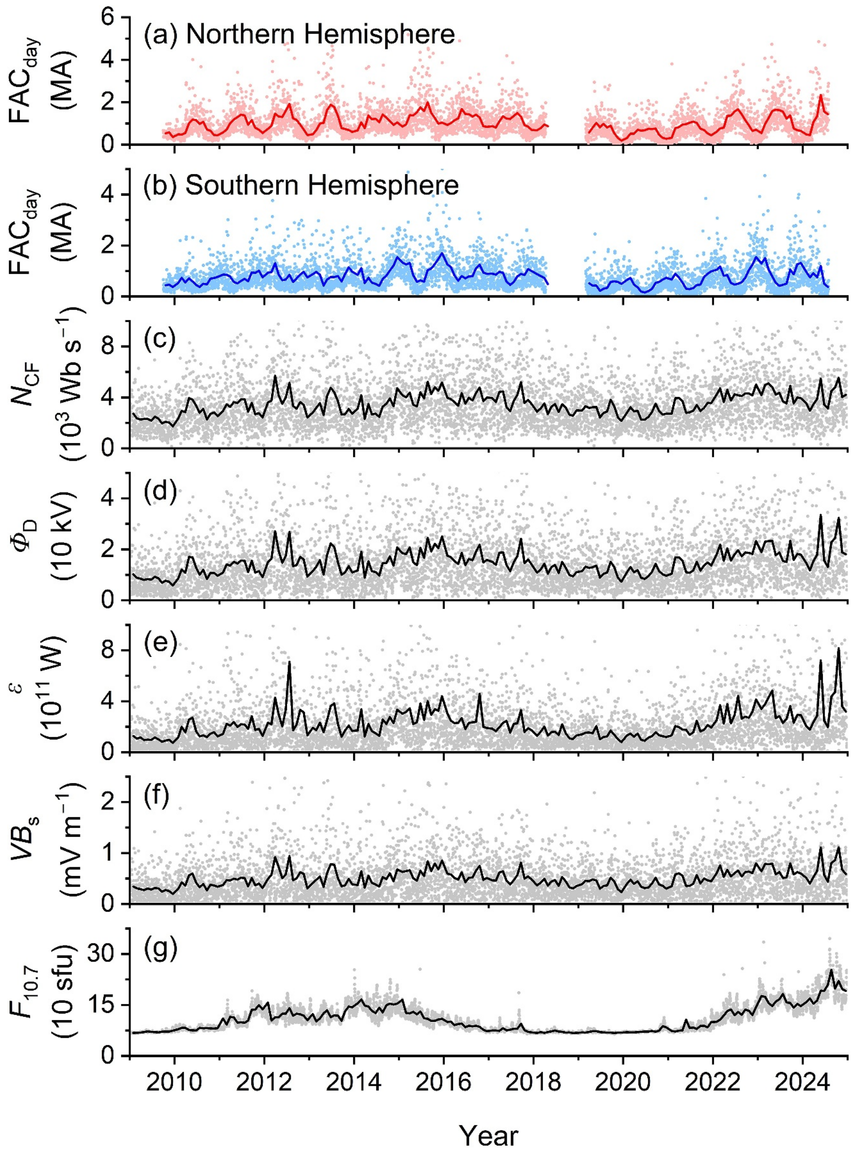

Figure 1. Variations of FACs and solar wind-magnetosphere energy coupling functions during 2009 through 2024. From top to bottom, the panels are (a) the northern hemispheric dayside FAC (FAC_{day}), (b) the southern hemispheric FAC_{day}, (c) the Newell coupling function N_{CF}, (d) the dayside magnetopause reconnection rate Φ_D, (e) the Akasofu ε-parameter, (f) the motional electric field VB_s, and (g) the $F_{10.7}$ solar flux. In each panel, filled circles indicate daily mean values, and solid lines indicate monthly mean values.

observed during years of high solar activity (2011–2015, 2022–2024) and low solar activity years (2009, 2010, 2016–2021) (see Appendix C, Figure C1 and Table C1).

Southern hemispheric FAC_{day} year-month contour is shown in Figure 2c. As expected, southern hemispheric winter months (May–July) are characterized by the weakest FAC_{day}, while southern hemispheric summer months (November-January) exhibit the strongest FAC_{day} values. However, on average, the northern hemispheric summer FAC_{day} is ~1.4 times the southern hemispheric summer FAC_{day}. The southern hemispheric summer (maximum)-to-winter (minimum) FAC_{day} ratio is ~2.0. The southern hemispheric FAC_{day} exhibits more or less similar solar cycle variation as the northern hemispheric FAC_{day}, with a peak during 2015, a minimum during 2019 (Figure 2h), and a peak-to-minimum ratio of ~2.6 (Appendix B, Table B1).

The year-month contours of nightside FACs (FAC_{night}) in the northern and southern hemispheres are shown in Figures 2e and 2f, respectively. They exhibit similar solar cycle profiles as in the FAC_{day}, exept that yearly mean

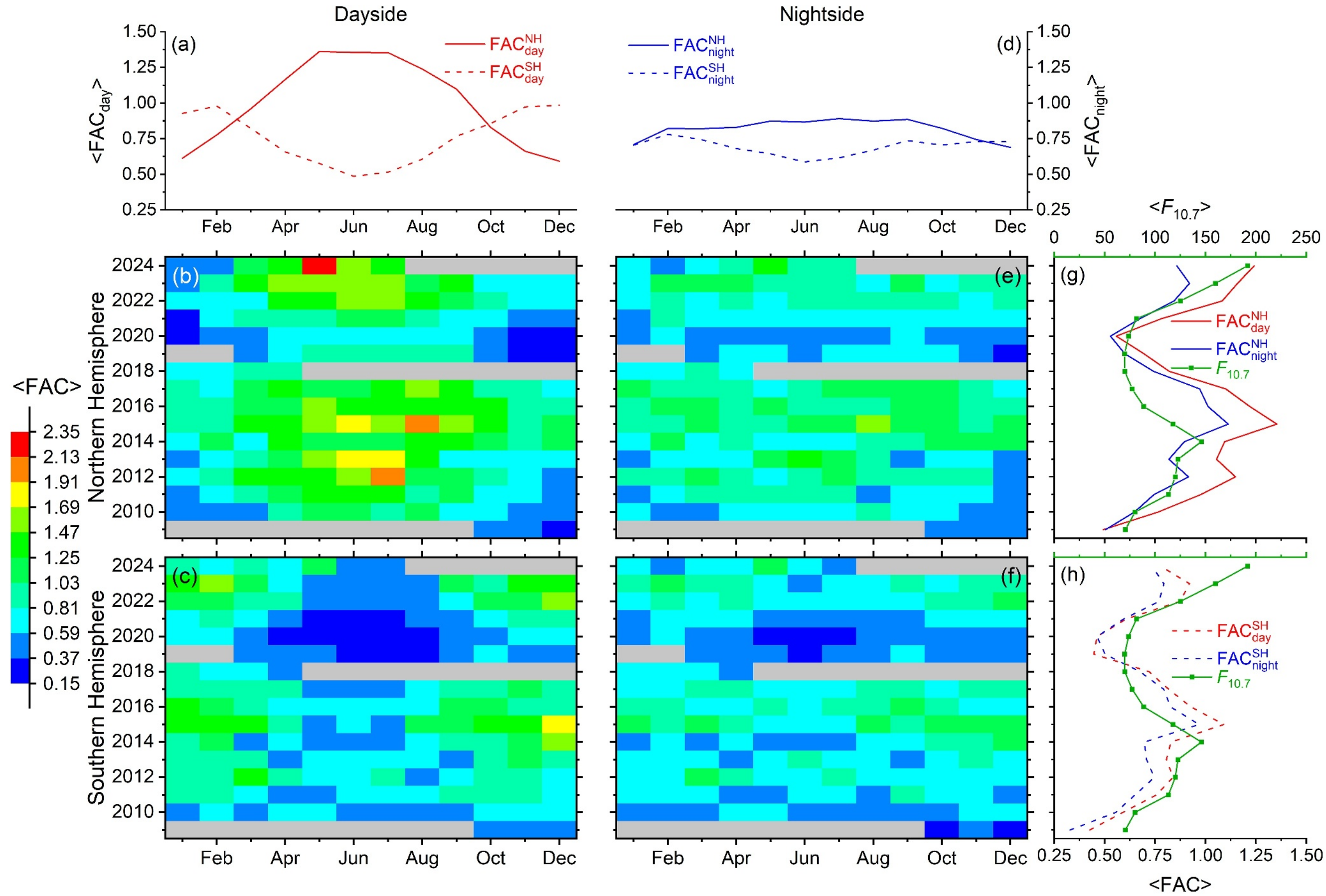

Figure 2. Seasonal and solar cycle variations of FACs. Contour plots (b, c, e, f) show year-month contours of monthly mean FACs. Different colors indicate FAC intensities as shown in the color bar at the left. Data gaps are marked by gray shadings. Top panels (a, d) show monthly mean FAC variations during different months. The right-hand panels (g, h) show yearly mean FAC and $F_{10.7}$ variations during different years. $FAC_{day}{}^{NH}$ and $FAC_{night}{}^{NH}$ ($FAC_{day}{}^{SH}$ and $FAC_{night}{}^{SH}$) indicate dayside and nightside FACs in the northern (southern) hemisphere, respectively. FACs are given in the unit of MA, and $F_{10.7}$ in the solar flux unit (sfu), where 1 sfu = 10^{-22} W m^{-2} Hz^{-1}.

FAC_{night} values are significantly lower than yearly mean FAC_{day} values, particularly during high solar activity periods (Figures 2g and 2h). The maximum-to-minimum yearly mean FAC_{night} ratio is ~2.2 for the northern hemisphere, and ~3.0 for the southern hemisphere (~120%–200% solar cycle varistions of FAC_{night}). However, the seasonal variations of FAC_{night} (Figure 2d) are significantly different than those of FAC_{day} (Figure 2a). In the northern hemisphere (Figure 2e), the FAC_{night} exhibits more or less similar values from February through October, with slightly lower values during winter months (Novenber-January). In the southern hemisphere (Figure 2f), May-July (sountern hemispheric winter) exhibit slightly lower FAC_{night} compared to other months. The summer-to-winter ratio for FAC_{night} is only ~1.3 (~30% variation), indicating weaker seasonal dependence of FAC_{night}.

An interesting feature of the day-night asymmetry is revealed from comparison of FACs in the summer and winter hemispheres. In the summer hemisphere, FAC_{day} is ~1.5 times (~50% stronger than) FAC_{night}. On the other hand, in the winter hemisphere, FAC_{night} is slightly stronger than FAC_{day}, by a factor of ~1.2 (~20%).

The seasonal variations are further studied by computations of statistical distributions of FACs. Figure 3 shows distributions of monthly mean FAC_{total}, FAC_{day}, and FAC_{night}, and the statistical results are summarized in Table 1. As clear from large 1-σ deviations (~26%–34% of the mean values), FACs exhibit a large range of variation. Considering medians of the non-normal distributions, FAC_{day} in the summer hemisphere is found to be ~99%, ~38%, and ~35% stronger than in the winter, spring, and fall hemispheres, respectively. The spring and fall hemispheric FAC_{day} median values are ~45%, and ~48% stronger than in the winter hemisphere,

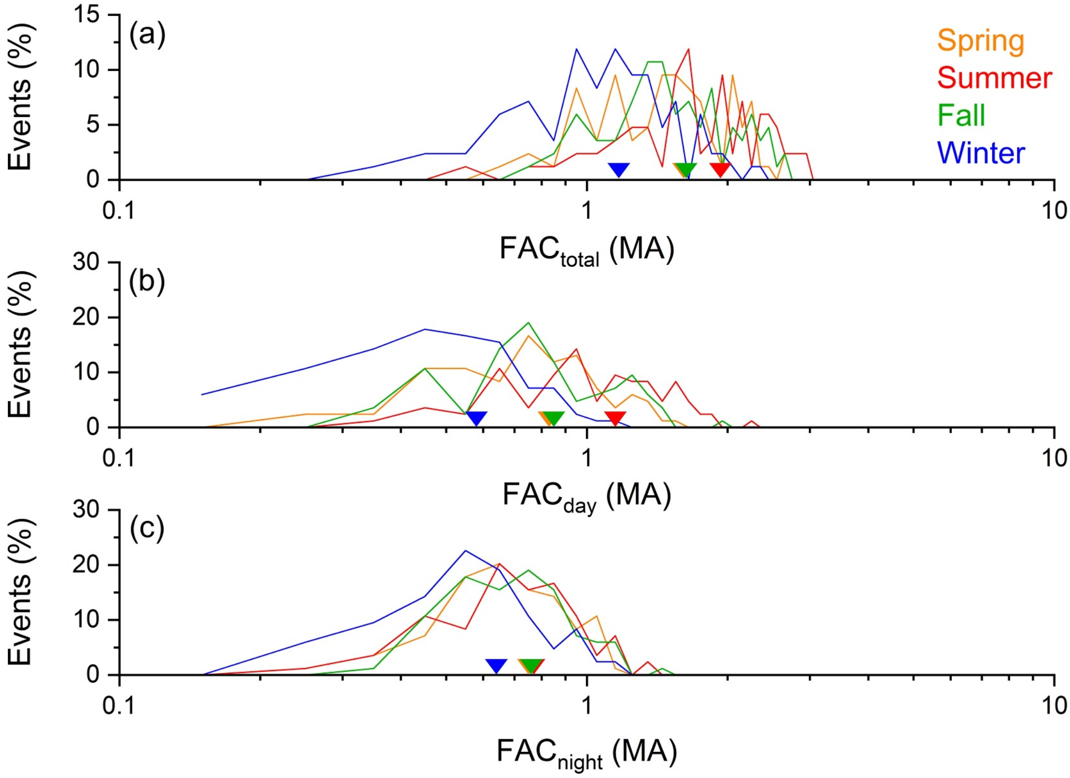

Figure 3. Distributions of the monthly mean (a) FAC$_{total}$, (b) FAC$_{day}$, and (c) FAC$_{night}$ for spring (orange), summer (red), fall (green), and winter (blue) hemispheric FAC measurements. Downward arrows indicate median values of the distributions.

respectively. However, the seasonal differences are significantly lower for FAC$_{night}$. Winter hemispheric FAC$_{night}$ is ∼17%, ∼16%, and ∼14% weaker than in the summer, fall, and spring hemispheres, respectively.

We also identified day-night asymmetries in FACs in each of the seasons. While FAC$_{day}$ is ∼49%, ∼12%, and ∼11% stronger than FAC$_{night}$ in summer, fall, and spring hemispheres, respectively, FAC$_{day}$ is ∼10% weaker than FAC$_{night}$ in the winter hemisphere.

Statistical significances of these seasonal and day-night variations have been confirmed by the statistical probability factor $p < 0.05$ (Press et al., 1992). Results presented in Figure 3 and Table 1 (considering medians of non-normal distributions) are consistent with those presented in Figures B1, C1, and 2, and Tables B1 and C1 (considering mean values). However, slight differences in the numbers (percentages) are due to the use of medians and mean values.

Figure 4 shows variations of monthly mean FACs with monthly mean values of the solar wind coupling functions. To assess the relationships between the parameters, we estimated the Spearman's rank correlation coefficients (r), which are listed in Table 2. While both FAC$_{day}$ and FAC$_{night}$ exhibit increasing trends with increases in the coupling functions (Figure 4), the correlation coefficients are prominently stronger for FAC$_{night}$ (r = 0.78–0.82) than for FAC$_{day}$ (r = 0.58–0.61). This result plausibly indicates that long-term variations of FAC$_{night}$ are "driven" by solar wind-magnetosphere coupling processes, while contribution of the energy coupling is slightly lesser on the FAC$_{day}$ variations (consistent with result obtained from Figure 1).

4. Discussion

We have used a ∼15-yearlong FAC database to study long-term variations of FACs. Both dayside and nightside FACs exhibit significant solar cycle phase dependence with the strongest FACs occurring ∼1 year after the solar cycle $F_{10.7}$ peak occurrence and the weakest FACs recorded ∼1 year after the solar cycle minimum. The yearly mean FAC maximum-to-minimum ratio is ∼2–3 in a solar cycle, indicative of large (∼100%–200%) FAC

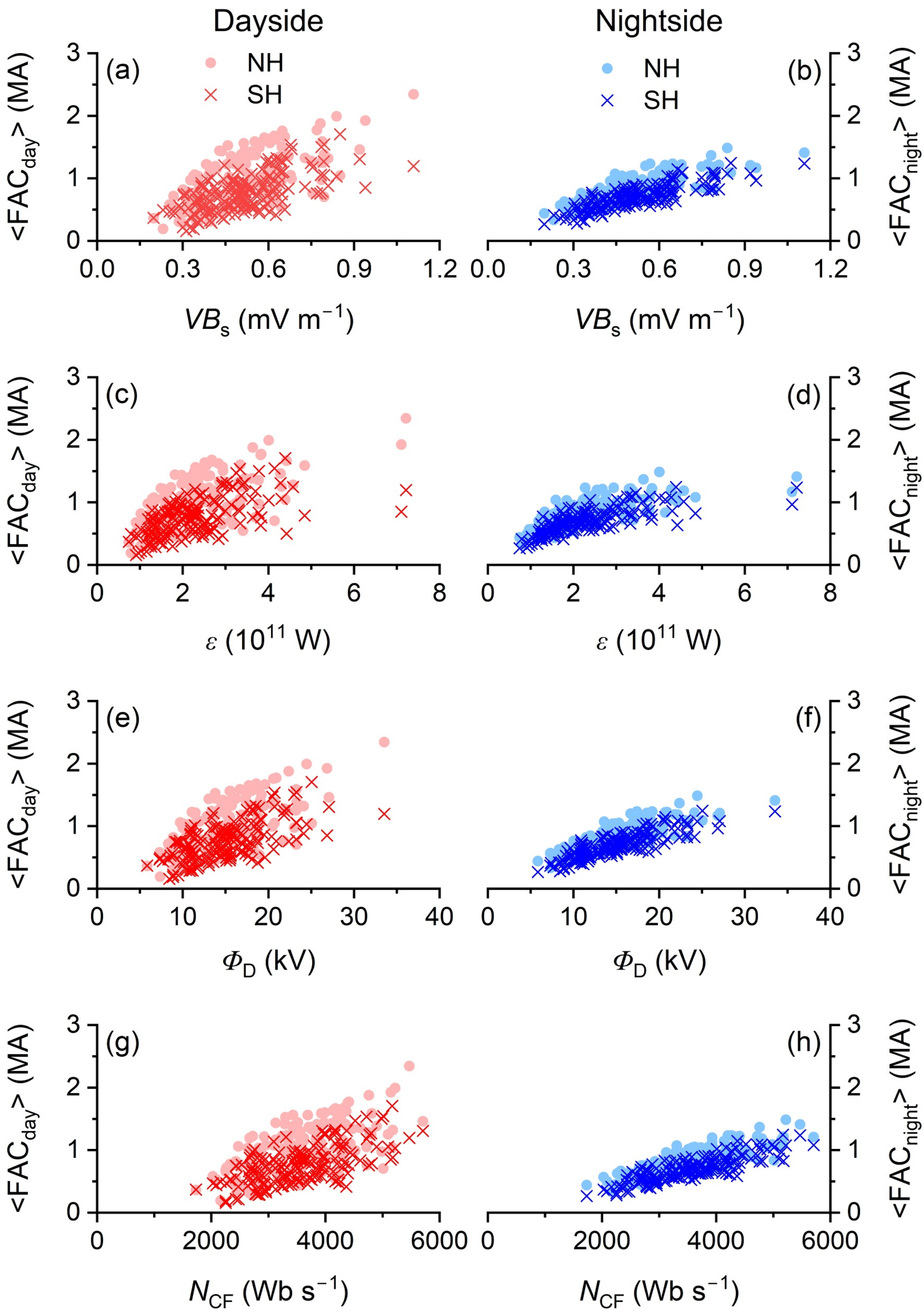

Figure 4. Statistical relationships of the FACs with solar wind-magnetosphere energy coupling functions. From top to bottom, the panels show variations of monthly mean FACs with monthly mean (a, b) VB_s, (c, d) ε, (e, f) Φ_D, and (g, h) N_{CF}. Left and right panels correspond to daytime and nighttime FACs, respectively. In each panel, filled circles and crosses correspond to northen and southern hemispheric FACs, respectively.

Table 1
Statistical Mean ± 1-σ Deviation (Median) of FAC Distributions Shown in Figure 3

	FAC_{total} (MA)	FAC_{day} (MA)	FAC_{night} (MA)
Spring	1.63 ± 0.47 (1.61)	0.86 ± 0.29 (0.83)	0.77 ± 0.20 (0.75)
Summer	1.96 ± 0.61 (1.93)	1.16 ± 0.39 (1.15)	0.80 ± 0.23 (0.77)
Fall	1.72 ± 0.52 (1.63)	0.93 ± 0.32 (0.85)	0.79 ± 0.22 (0.76)
Winter	1.24 ± 0.42 (1.17)	0.57 ± 0.22 (0.58)	0.67 ± 0.21 (0.64)

variability induced by solar and solar wind activities. The solar cycle variation is observed for both dayside and nightside FACs in all seasons. Such a solar cycle dependence of FACs is reported for the first time, to our knowledge. The descending phase of the solar cycle is characterized by enhanced FACs. This latter result may be associated with substorm and convection events driven by solar wind high-speed streams (HSSs; Neugebauer & Snyder, 1966; Phillips et al., 1995; Tsurutani et al., 2006) emanated from solar coronal holes (Krieger et al., 1973), which are encountered by Earth more frequently during the descending phase when the coronal holes expand in size and move equatorwad on the sun (Tsurutani et al., 1995; Tsurutani, Gonzalez, et al., 2006; Tsurutani, McPherron, et al., 2006). Previous studies have shown higher occurrences of isolated substorms (Tanskanen, 2009; Tanskanen et al., 2011) as well as of intense substorm clusters continuing for several days (Hajra et al., 2013; Tsurutani & Gonzalez, 1987) during the descending phase. Latter events are called high-intensity long-duration continuous auroral electrojet (AE) activities (HILDCAAs; Tsurutani & Gonzalez, 1987), which are caused by HSS Alfvén waves.

We observed a summer-to-winter ratio of ∼2–2.3 for dayside monthly mean FACs and ∼1.3 for nightside FACs. Based on the FAC distributions (median values) during different seasons, dayside current in the summer hemisphere is ∼99% stronger than in the winter hemisphere, and ∼35%–38% stronger than in the equinoxes. Nightside current in the winter hemisphere is only ∼14%–17% weaker than in other seasons. The numbers indicate strong seasonal variation of dayside FACs and weaker seasonal depence of nightside FACs. These quantitative results are consistent with results presented by Fujii et al. (1981) based on ∼4 years of TRIAD spacecraft observations of northern hemispheric currents, and with the Coxon et al. (2016) results based on ∼6 years of AMPERE FAC measurements in both hemispheres. What is new in this present study is that using ∼15 years of database, we were able to find year-to-year or solar cycle phase variation of the seasonal dependences (not done in previous works based on shorter databases). It is found that the summer-winter asymmetry of dayside FACs and lack of the same (or weaker asymmetry) for nightside FACs are consistent for all years or solar activity levels, with only slight variations in the intensities. A clear hemispheric asymmetry is noted in terms of a ∼1.4 factor stronger dayside FACs in the northern summer than in the southern summer. We recommend Coxon et al. (2016) for an extensive discussion of the hemispheric asymmetry in the current intensities in the context of reported hemispheric asymmetries in ionospheric electron densities (Tulunay & Grebowsky, 1987) and total electron content (Clausen & Moen, 2015), which are closely related to ionospheric conductance, in ionospheric convection velocities (Förster et al., 2007), in cross-polar cap potential (Förster & Haaland, 2015), in ion drift velocities and high-latitude neutral wind vortices at dawn and dusk, attributed to asymmetries in the geomagnetic fields (Cnossen & Förster, 2016).

Another interesting and new result is a varying day-night asymmetry between summer and winter hemispheres. While dayside FACs are, on average, ∼1.5 times nightside FACs in the summer hemisphere, nightside FACs are stronger (by a factor of ∼1.2) than dayside FACs in the winter hemisphere. Dayside FACs being stronger than nightside FACs in the summer hemisphere is consistent with variation of ionospheric conductance between day and night. However, nightside FACs being stronger than dayside FACs in the winter hemisphere is inconsistent with the solar illumination-induced conductance variation hypothesis. Is this result related to much cumulative currents during longer-duration winter nights than shorter days? Or, is it due to stronger influence of solar wind energy flow (higher correlation with solar wind-magnetosphere coupling functions) during nights as observed in this work? Recent studies (Wang & Lühr, 2023; Wang et al., 2024; Zhong et al., 2022) indicated that energetic

Table 2
Spearman's Rank Correlation Coefficients (r) Between Monthly Mean FACs and Solar Wind-Magnetosphere Coupling Functions Shown in Figure 4

	FAC_{day}		FAC_{night}	
	Northern Hemisphere	Southern Hemisphere	Northern Hemisphere	Southern Hemisphere
VB_s	0.58	0.59	0.79	0.80
ε	0.61	0.59	0.78	0.78
Φ_D	0.61	0.60	0.82	0.82
N_{CF}	0.60	0.59	0.82	0.80

Note. The correlation coefficnets are significant at >99.9% confidence level, as confirmed by Student's *t*-test (Student, 1908).

particle precipitation associated with substorms may enhance the auroral ionospheric Hall conductance during nighttime, possibly contributing to enhanced nightside FACs in the winter hemisphere. However, this hypothesis should be tested by furture studies.

We found that dayside FACs, largely controlled by ionospheric conductance, exhibit a clear and strong seasonal dependence, while nightside FACs with lesser influence of ionospheric conductance are strongly correlated to the solar wind-magnetosphere energy coupling processes. In other words, long-term trends of dayside and nightside FACs are plausibly driven by two different mechanisms, ionospheric conductance and solar wind-magnetosphere energy coupling, respectively, or relative contributions of these two factors vary between day and night. In addition, the nightside current system should also be modulated by substorm activity and the flux-integrated conductivity in both hemispheres (Wang & Lühr, 2021, 2023). These results should be implemented in any modeling efforts for FACs. The quantitative results presented in this work may be useful in developing predictive FAC models.

Appendix A: Lomb-Scargle Periodograms

Figure A1 shows Lomb-Scargle periodograms of monthly mean dayside field-aligned currents (FACs) in the northern and southern hemispheres. These are characterized by clear peaks in the spectral power at a ∼12-month period. This result is a clear indicative of annual variation of dayside FACs.

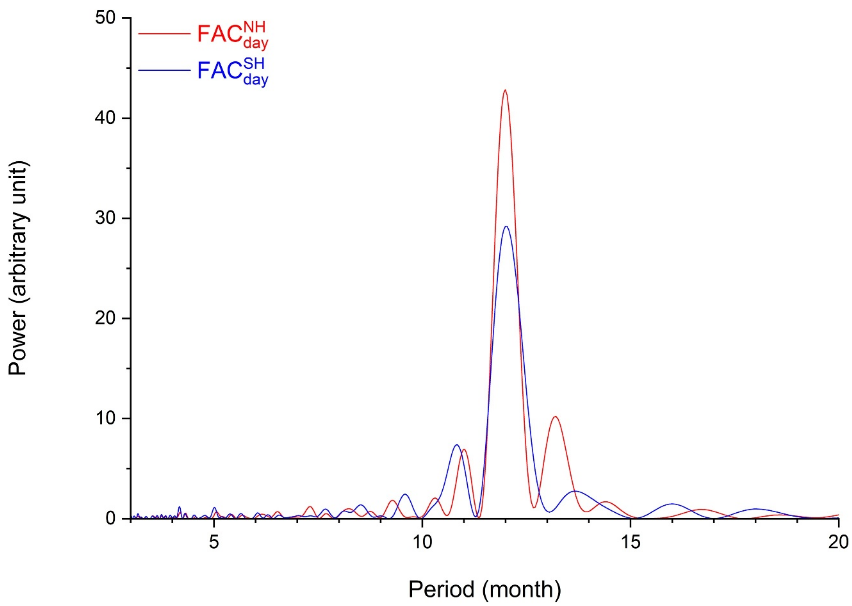

Figure A1. Lomb-Scargle periodograms of northern and southern hemispheric dayside FACs, indicated by $FAC_{day}{}^{NH}$ and $FAC_{day}{}^{SH}$, respectively. Clear peaks are observed in power for a period of ∼12 months.

Appendix B: Solar Cycle Variations

Figure B1 shows variations of yearly mean FACs for all months combined as well as separately for different seasons. Variation of $F_{10.7}$ solar flux is included to compare the FAC variations with solar activity cycle. FAC variations are characterized by a peak intensity ∼1 year after the $F_{10.7}$ peak and a minimum ∼1 year after the $F_{10.7}$ minimum. The maximum-to-minimum ratios in the yearly mean FAC variations are listed in Table B1. The ratio varies between ∼1.9 and ∼4.1, indicating large solar cycle variations of ∼90%–310%. While the FAC solar cycle variation is observed in both hemispheres, for both day and night, and during all seasons, we note slight variation in the ratio during different seasons.

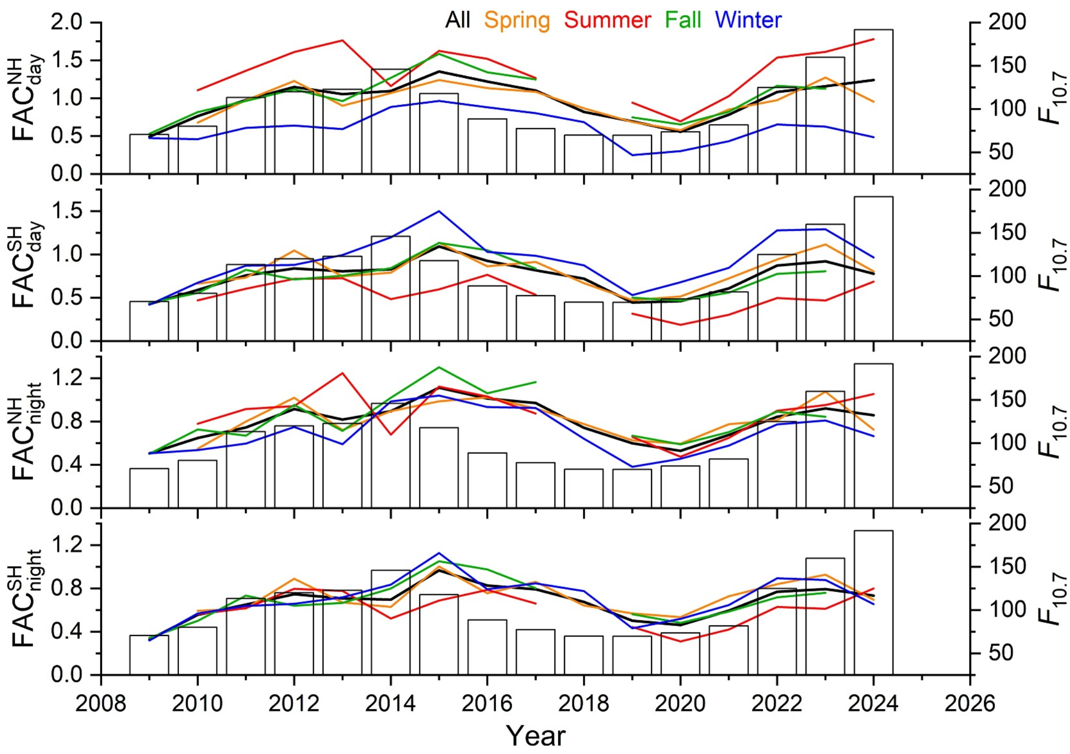

Figure B1. Variations of yearly mean FACs for all months (black), spring (orange), summer (red), fall (green), and winter (blue) seasons (lines, legend on the left) and $F_{10.7}$ solar fluxes (histogram, legend on the right). From top to bottom, the panels correspond to FAC_{day} in the northern and southern hemispheres, and FAC_{night} in the northern and southern hemispheres, respectively.

Table B1
The Maximum-to-Minimum Ratios in Yearly Mean FAC Variations for All Months and During Different Seasons Shown in Figure B1

	All	Spring	Summer	Fall	Winter
FAC_{day}^{NH}	2.7	2.2	2.6	3.0	3.9
FAC_{day}^{SH}	2.6	2.4	4.1	2.6	3.6
FAC_{night}^{NH}	2.2	2.0	2.6	2.6	2.7
FAC_{night}^{SH}	3.0	1.9	2.6	3.1	3.5

Appendix C: Seasonal Variations

Figure C1 shows variations of monthly mean FACs for all years and years of low (2009, 2010, 2016–2021) and high (2011–2015, 2022–2024) solar activities. Based on this analysis, we computed summer maximum to winter minimum FAC intensity ratios in order to quantify the summer-winter asymmetry in FACs. The ratios are listed in Table C1. The ratio varies between ~2.0 and 2.5 for FAC_{day} and between ~1.3 and ~1.5 for FAC_{night}, indicating strong (~100%–150%) summer-winter asymmetry for FAC_{day} and weaker (~30%–50%) asymmetry for FAC_{night}. This seems to be consistent at different solar activity phases.

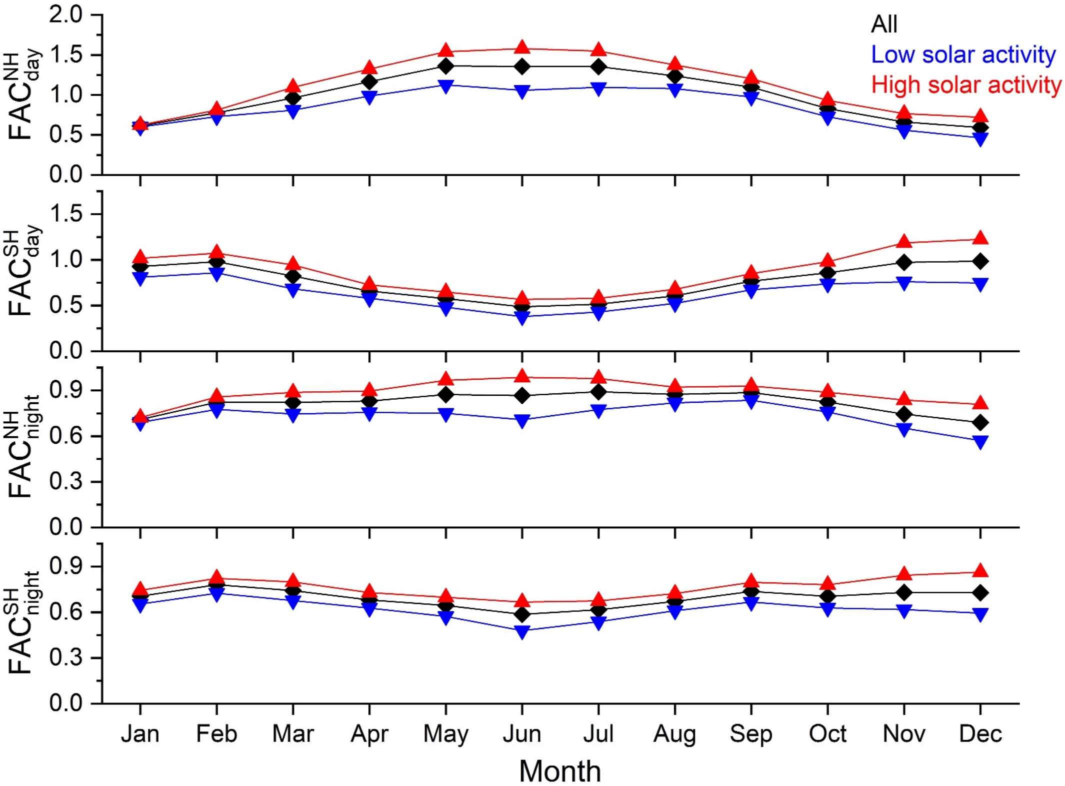

Figure C1. Variations of monthly mean FACs for all years (black) and years of low solar activity (2009, 2010, 2016–2021, blue), and high solar activity (2011–2015, 2022–2024, red). From top to bottom, the panels correspond to FAC_{day} in northern and southern hemispheres, and FAC_{night} in northern and southern hemispheres, respectively.

Table C1
The Summer-to-Winter Ratios in Monthly Mean FACs for All Years and During Years of Low (2009, 2010, 2016–2021) and High (2011–2015, 2022–2024) Solar Activities Shown in Figure C1

	All	Low solar activity	High solar activity
FAC_{day}^{NH}	2.3	2.4	2.5
FAC_{day}^{SH}	2.0	2.3	2.2
FAC_{night}^{NH}	1.3	1.5	1.4
FAC_{night}^{SH}	1.3	1.5	1.3

Conflict of Interest

The authors declare no conflicts of interest relevant to this study.

Data Availability Statement

The FAC data are obtained from the AMPERE Science Data Center of the Johns Hopkins Applied Physics Laboratory (https://ampere.jhuapl.edu/). The data is free to download from the download page under the AMPERE Derived Product Data Files (Daily) (https://ampere.jhuapl.edu/download/?page=derivedProductsTab). The near-Earth solar wind plasma and IMF data are obtained from NASA's OMNIWeb Plus database (https://omniweb.gsfc.nasa.gov/). The high-resolution data can be directly downloaded from the page: https://omniweb.gsfc.nasa.gov/form/omni_min.html, by specifying start and stop times. The $F_{10.7}$ solar fluxes are obtained from the Laboratory for Atmospheric and Space Physics (LASP) Interactive Solar Irradiance Data Center (https://lasp.colorado.edu/lisird/).

Acknowledgments
The work of R. H. is funded by the "Hundred Talents Program" of the Chinese Academy of Sciences (CAS), and the Excellent Young Scientists Fund Program (Overseas) of the National Natural Science Foundation of China (NSFC). We would like to thank the reviewers for extremely valuable suggestions that substantially improved the manuscript.

References

Anderson, B. J., Angappan, R., Barik, A., Vines, S. K., Stanley, S., Bernasconi, P. N., et al. (2021). Iridium communications satellite constellation data for study of Earth's magnetic field. *Geochemistry, Geophysics, Geosystems*, *22*(8), e2020GC009515. https://doi.org/10.1029/2020GC009515

Anderson, B. J., Takahashi, K., Kamei, T., Waters, C. L., & Toth, B. A. (2002). Birkeland current system key parameters derived from Iridium observations: Method and initial validation results. *Journal of Geophysical Research*, *107*(A6), SMP11-1–SMP11-13. https://doi.org/10.1029/2001JA000080

Birkeland, K. (1908). *The Norwegian Aurora Polaris Expedition, 1902–1903* (Vol. 1). Christiania: H. Aschelhoug. https://doi.org/10.5962/bhl.title.17857

Birkeland, K. (1913). *The Norwegian Aurora Polaris Expedition 1902–1903* (Vol. 2). Christiania: H. Aschelhoug.

Burton, R. K., McPherron, R. L., & Russell, C. T. (1975). An empirical relationship between interplanetary conditions and *Dst*. *Journal of Geophysical Research*, *80*(31), 4204–4214. https://doi.org/10.1029/JA080i031p04204

Chapman, S., & Ferraro, V. C. A. (1931). A new theory of magnetic storms. *Terrestrial Magnetism and Atmospheric Electricity*, *36*(2), 77–97. https://doi.org/10.1029/TE036i002p00077

Clausen, L. B. N., & Moen, J. I. (2015). Electron density enhancements in the polar cap during periods of dayside reconnection. *Journal of Geophysical Research: Space Physics*, *120*(6), 4452–4464. https://doi.org/10.1002/2015JA021188

Cnossen, I., & Förster, M. (2016). North-south asymmetries in the polar thermosphere-ionosphere system: Solar cycle and seasonal influences. *Journal of Geophysical Research: Space Physics*, *121*(1), 612–627. https://doi.org/10.1002/2015JA021750

Coxon, J. C., Milan, S. E., Carter, J. A., Clausen, L. B. N., Anderson, B. J., & Korth, H. (2016). Seasonal and diurnal variations in AMPERE observations of the Birkeland currents compared to modeled results. *Journal of Geophysical Research: Space Physics*, *121*(5), 4027–4040. https://doi.org/10.1002/2015JA022050

Coxon, J. C., Milan, S. E., Clausen, L. B. N., Anderson, B. J., & Korth, H. (2014a). A superposed epoch analysis of the regions 1 and 2 Birkeland currents observed by AMPERE during substorms. *Journal of Geophysical Research: Space Physics*, *119*(12), 9834–9846. https://doi.org/10.1002/2014JA020500

Coxon, J. C., Milan, S. E., Clausen, L. B. N., Anderson, B. J., & Korth, H. (2014b). The magnitudes of the regions 1 and 2 Birkeland currents observed by AMPERE and their role in solar wind-magnetosphere-ionosphere coupling. *Journal of Geophysical Research: Space Physics*, *119*(12), 9804–9815. https://doi.org/10.1002/2014JA020138

Crooker, N. U., & McPherron, R. L. (1972). On the distinction between the auroral electrojet and partial ring current systems. *Journal of Geophysical Research*, *77*(34), 6886–6889. https://doi.org/10.1029/JA077i034p06886

Cummings, W. D. (1966). Asymmetric ring currents and the low-latitude disturbance daily variation. *Journal of Geophysical Research*, *71*(19), 4495–4503. https://doi.org/10.1029/JZ071i019p04495

Cummings, W. D., & Dessler, A. J. (1967). Field-aligned currents in the magnetosphere. *Journal of Geophysical Research*, *72*(3), 1007–1013. https://doi.org/10.1029/JZ072i003p01007

Finch, I. D., Lockwood, M. L., & Rouillard, A. P. (2008). Effects of solar wind magnetosphere coupling recorded at different geomagnetic latitudes: Separation of directly-driven and storage/release systems. *Geophysical Research Letters*, *35*(21), 2008GL035399. https://doi.org/10.1029/2008GL035399

Förster, M., & Haaland, S. (2015). Interhemispheric differences in ionospheric convection: Cluster EDI observations revisited. *Journal of Geophysical Research: Space Physics*, *120*(7), 5805–5823. https://doi.org/10.1002/2014JA020774

Förster, M., Paschmann, G., Haaland, S. E., Quinn, J. M., Torbert, R. B., Vaith, H., & Kletzing, C. A. (2007). High-latitude plasma convection from Cluster EDI: Variances and solar wind correlations. *Annales Geophysicae*, *25*(7), 1691–1707. https://doi.org/10.5194/angeo-25-1691-2007

Fujii, R., Iijima, T., Potemra, T. A., & Sugiura, M. (1981). Seasonal dependence of large-scale Birkeland currents. *Geophysical Research Letters*, *8*(10), 1103–1106. https://doi.org/10.1029/GL008i010p01103

Fukushima, N., & Kamide, Y. (1973). Partial ring current models for worldwide geomagnetic disturbances. *Reviews of Geophysics*, *11*(4), 795–853. https://doi.org/10.1029/RG011i004p00795

Gibbons, J. D., & Chakraborti, S. (2011). Nonparametric statistical inference. In M. Lovric (Ed.), *International Encyclopedia of Statistical Science* (pp. 977–979). Springer Berlin Heidelberg. https://doi.org/10.1007/978-3-642-04898-2_420

Hajra, R., Echer, E., Tsurutani, B. T., & Gonzalez, W. D. (2013). Solar cycle dependence of High-Intensity Long-Duration Continuous AE Activity (HILDCAA) events, relativistic electron predictors? *Journal of Geophysical Research: Space Physics*, *118*(9), 5626–5638. https://doi.org/10.1002/jgra.50530

Hajra, R., Tsurutani, B. T., Lakhina, G. S., Lu, Q., & Du, A. (2024). Interplanetary causes and impacts of the 2024 May superstorm on the geosphere: An overview. *The Astrophysical Journal*, *974*(2), 264. https://doi.org/10.3847/1538-4357/ad7462

Hajra, R., Tsurutani, B. T., Lu, Q., Horne, R. B., Lakhina, G. S., Yang, X., et al. (2024). The April 2023 SYM-H = −233 nT geomagnetic storm: A classical event. *Journal of Geophysical Research: Space Physics*, *129*(10), e2024JA032986. https://doi.org/10.1029/2024JA032986

Iijima, T., & Potemra, T. A. (1976a). Field-aligned currents in the dayside cusp observed by Triad. *Journal of Geophysical Research*, *81*(34), 5971–5979. https://doi.org/10.1029/JA081i034p05971

Iijima, T., & Potemra, T. A. (1976b). The amplitude distribution of field-aligned currents at northern high latitudes observed by Triad. *Journal of Geophysical Research*, *81*(13), 2165–2174. https://doi.org/10.1029/JA081i013p02165

Iijima, T., & Potemra, T. A. (1978). Large-scale characteristics of field-aligned currents associated with substorms. *Journal of Geophysical Research*, *83*(A2), 599–615. https://doi.org/10.1029/JA083iA02p00599

King, J. H., & Papitashvili, N. E. (2020). OMNI 1-min data set [Dataset]. *NASA Space Physics Data Facility*. https://doi.org/10.48322/45BB-8792

Krieger, A. S., Timothy, A. F., & Roelof, E. C. (1973). A coronal hole and its identification as the source of a high velocity solar wind stream. *Solar Physics*, *29*(2), 505–525. https://doi.org/10.1007/bf00150828

Lomb, N. R. (1976). Least-squares frequency analysis of unequally spaced data. *Astrophysics and Space Science*, *39*(2), 447–462. https://doi.org/10.1007/BF00648343

Milan, S. E., Gosling, J. S., & Hubert, B. (2012). Relationship between interplanetary parameters and the magnetopause reconnection rate quantified from observations of the expanding polar cap. *Journal of Geophysical Research*, *117*(A3), 2011JA017082. https://doi.org/10.1029/2011JA017082

Ness, N. F. (1965). The Earth's magnetic tail. *Journal of Geophysical Research*, *70*(13), 2989–3005. https://doi.org/10.1029/JZ070i013p02989

Neugebauer, M., & Snyder, C. W. (1966). Mariner 2 observations of the solar wind: 1. Average properties. *Journal of Geophysical Research*, *71*(19), 4469–4484. https://doi.org/10.1029/jz071i019p04469

Newell, P. T., Sotirelis, T., Liou, K., Meng, C.-I., & Rich, F. J. (2007). A nearly universal solar wind-magnetosphere coupling function inferred from 10 magnetospheric state variables. *Journal of Geophysical Research*, *112*(A1), 2006JA012015. https://doi.org/10.1029/2006JA012015

Pedersen, M. N., Vanhamäki, H., Aikio, A. T., Käki, S., Workayehu, A. B., Waters, C. L., & Gjerloev, J. W. (2021). Field-aligned and ionospheric currents by AMPERE and SuperMAG during HSS/SIR-driven storms. *Journal of Geophysical Research: Space Physics*, *126*(11), e2021JA029437. https://doi.org/10.1029/2021JA029437

Pedersen, M. N., Vanhamäki, H., Aikio, A. T., Waters, C. L., Gjerloev, J. W., Käki, S., & Workayehu, A. B. (2022). Effect of ICME-driven storms on field-aligned and ionospheric currents from AMPERE and SuperMAG. *Journal of Geophysical Research: Space Physics*, *127*(8), e2022JA030423. https://doi.org/10.1029/2022JA030423

Perreault, P., & Akasofu, S.-I. (1978). A study of geomagnetic storms. *Geophysical Journal International*, *54*(3), 547–573. https://doi.org/10.1111/j.1365-246X.1978.tb05494.x

Phillips, J. L., Bame, S. J., Feldman, W. C., Gosling, J. T., Hammond, C. M., McComas, D. J., et al. (1995). Ulysses solar wind plasma observations at high southerly latitudes. *Science*, *268*(5213), 1030–1033. https://doi.org/10.1126/science.268.5213.1030

Press, W. H., Teukolsky, S. A., Vetterling, W. T., & Flannery, B. P. (1992). *Numerical Recipes: The Art of Scientific Computing* (2nd ed.). Cambridge University Press.

Reiff, P. H. (1990). The use and misuse of statistics in space physics. *Journal of Geomagnetism and Geoelectricity*, *42*(9), 1145–1174. https://doi.org/10.5636/jgg.42.1145

Scargle, J. D. (1982). Studies in astronomical time series analysis. II—Statistical aspects of spectral analysis of unevenly spaced data. *The Astrophysical Journal*, *263*, 835. https://doi.org/10.1086/160554

Speiser, T. W., & Ness, N. F. (1967). The neutral sheet in the geomagnetic tail: Its motion, equivalent currents, and field line connection through it. *Journal of Geophysical Research*, *72*(1), 131. https://doi.org/10.1029/JZ072i001p00131

Student. (1908). The probable error of a mean. *Biometrika*, *6*(1), 1. https://doi.org/10.2307/2331554

Tanskanen, E. I. (2009). A comprehensive high-throughput analysis of substorms observed by IMAGE magnetometer network: Years 1993–2003 examined. *Journal of Geophysical Research*, *114*(A5), 2008JA013682. https://doi.org/10.1029/2008JA013682

Tanskanen, E. I., Pulkkinen, T. I., Viljanen, A., Mursula, K., Partamies, N., & Slavin, J. A. (2011). From space weather toward space climate time scales: Substorm analysis from 1993 to 2008: Space climate. *Journal of Geophysical Research*, *116*(A5), A00I34. https://doi.org/10.1029/2010JA015788

Tsurutani, B. T., & Gonzalez, W. D. (1987). The cause of High-Intensity Long-Duration Continuous AE Activity (HILDCAAs): Interplanetary Alfvén wave trains. *Planetary and Space Science*, *35*(4), 405–412. https://doi.org/10.1016/0032-0633(87)90097-3

Tsurutani, B. T., Gonzalez, W. D., Gonzalez, A. L. C., Guarnieri, F. L., Gopalswamy, N., Grande, M., et al. (2006). Corotating solar wind streams and recurrent geomagnetic activity: A review. *Journal of Geophysical Research*, *111*(A7), 2005JA011273. https://doi.org/10.1029/2005JA011273

Tsurutani, B. T., Gonzalez, W. D., Gonzalez, A. L. C., Tang, F., Arballo, J. K., & Okada, M. (1995). Interplanetary origin of geomagnetic activity in the declining phase of the solar cycle. *Journal of Geophysical Research*, *100*(A11), 21717–21733. https://doi.org/10.1029/95JA01476

Tsurutani, B. T., Gonzalez, W. D., Tang, F., & Lee, Y. T. (1992). Great magnetic storms. *Geophysical Research Letters*, *19*(1), 73–76. https://doi.org/10.1029/91GL02783

Tsurutani, B. T., McPherron, R. L., Gonzalez, W. D., Lu, G., Gopalswamy, N., & Guarnieri, F. L. (2006). Magnetic storms caused by corotating solar wind streams. In B. Tsurutani, R. McPherron, W. Gonzalez, G. Lu, J. H. A. Sobral, & N. Gopalswamy (Eds.), *Geophysical Monograph Series* (Vol. 167, pp. 1–17). American Geophysical Union. https://doi.org/10.1029/167GM03

Tulunay, Y. K., & Grebowsky, J. M. (1987). Hemispheric differences in the morphology of the high latitude ionosphere measured at ∼500 km. *Planetary and Space Science*, *35*(6), 821–826. https://doi.org/10.1016/0032-0633(87)90043-2

Wang, H., Cheng, Q., Lühr, H., Zhong, Y., Zhang, K., & Xia, H. (2024). Local time and hemispheric asymmetries of field-aligned currents and polar electrojet during May 2024 superstorm periods. *Journal of Geophysical Research: Space Physics*, *129*(11), e2024JA033020. https://doi.org/10.1029/2024JA033020

Wang, H., & Lühr, H. (2021). Effects of solar illumination and substorms on auroral electrojets based on CHAMP observations. *Journal of Geophysical Research: Space Physics*, *126*(2), e2020JA028905. https://doi.org/10.1029/2020JA028905

Wang, H., & Lühr, H. (2023). Magnetic longitudinal and local time variations of polar electrojet and field-aligned currents. *Journal of Geophysical Research: Space Physics*, *128*(10), e2023JA031874. https://doi.org/10.1029/2023JA031874

Wang, H., Lühr, H., & Ma, S. Y. (2005). Solar zenith angle and merging electric field control of field-aligned currents: A statistical study of the Southern Hemisphere. *Journal of Geophysical Research*, *110*(A3), 2004JA010530. https://doi.org/10.1029/2004JA010530

Wang, H., Lühr, H., Ma, S. Y., Weygand, J., Skoug, R. M., & Yin, F. (2006). Field-aligned currents observed by CHAMP during the intense 2003 geomagnetic storm events. *Annales Geophysicae*, *24*(1), 311–324. https://doi.org/10.5194/angeo-24-311-2006

Waters, C. L., Anderson, B. J., Green, D. L., Korth, H., Barnes, R. J., & Vanhamäki, H. (2020). Science data products for AMPERE. In M. W. Dunlop & H. Lühr (Eds.), *Ionospheric Multi-Spacecraft Analysis Tools* (pp. 141–165). Springer International Publishing. https://doi.org/10.1007/978-3-030-26732-2_7

Waters, C. L., Anderson, B. J., & Liou, K. (2001). Estimation of global field aligned currents using the iridium® System magnetometer data. *Geophysical Research Letters*, *28*(11), 2165–2168. https://doi.org/10.1029/2000GL012725

Zhong, Y., Wang, H., Zhang, K., Xia, H., & Qian, C. (2022). Local time response of auroral electrojet during magnetically disturbed periods: DMSP and CHAMP coordinated observations. *Journal of Geophysical Research: Space Physics*, *127*(8), e2022JA030624. https://doi.org/10.1029/2022JA030624

Zmuda, A. J., Martin, J. H., & Heuring, F. T. (1966). Transverse magnetic disturbances at 1100 kilometers in the auroral region. *Journal of Geophysical Research*, *71*(21), 5033–5045. https://doi.org/10.1029/JZ071i021p05033